Dielectric properties of ultrathin metal films around the percolation threshold

Martin Hövel, Bruno Gompf, and Martin Dressel
Physikalisches Institut, Universität Stuttgart, Pfaffenwaldring 57, 70550 Stuttgart, Germany
(Received 8 December 2009; published 5 January 2010)

Optical reflection measurements of thin Au films at and around the percolation threshold (film thickness 3–10 nm) are performed in an extremely broad spectral range up to 35 000 cm^{-1}. Combining spectroscopic ellipsometry, Fourier-transform infrared spectroscopy, and dc measurements, the dielectric properties of the films can be described over the whole frequency range by Kramers-Kronig consistent effective dielectric functions. The optical conductivity of the films is dominated by two contributions: a Drude component starting at the percolation threshold in the low-frequency range and by plasmons in the near-infrared region, which shift down in frequency with increasing film thickness. The interplay of both components leads to a dielectric anomaly in the infrared region with a maximum of the dielectric constant at the insulator-to-metal transition. The results are compared to predictions from effective-medium approximations and percolation theory.

DOI: 10.1103/PhysRevB.81.035402 PACS number(s): 73.50.−h, 71.30.+h, 73.25.+i, 78.20.Ci

I. INTRODUCTION

Although for many applications closed metal films as thin as possible are desired, the dielectric properties of percolating metal films around the insulator-to-metal transition are not well understood. Thick continuous metal films show a behavior similar to bulk material[1] and can therefore be well described by the Drude model when corrections for size effects are considered.[2,3] With decreasing thickness, the films become granular and below the percolation threshold, the metallic behavior disappears as far as the electrical transport is concerned. In principle, one can try to simulate the optical properties of semicontinues metal films with effective-medium approximation (EMA) theories.[4,5] The problem with EMA theories is that they are on one hand in contradiction with percolation theory.[6] In the Bruggeman approach, for example, exists a strong correlation between the particle shape and the percolation threshold, whereas in percolation theories the critical parameters are independent on the specific morphology.[7] On the other hand, it was also experimentally shown that they fail to describe the dielectric properties of ultrathin metal films.[8,9] Interestingly, the metal-to-insulator transition region has not yet been studied in detail over a broad-frequency range; nevertheless, these investigations should eventually provide the data to link the abrupt change in dc conductivity with the observed shift of plasmon resonances in the visible.

On the low-frequency side of the electromagnetic spectrum, percolation theories deal with an "idealized" dc conductivity or the electrical behavior at audio and radio frequencies up to some MHz.[7] On the other side of the spectrum—in the visible and ultraviolet—a large number of investigations has been carried out to understand the optical properties of arrays of clusters at surfaces.[10,11] In between, however—in the infrared and far-infrared spectral regions—little has been done so far. Here we report on Fourier-transform infrared reflection spectroscopy, spectroscopic ellipsometry, and dc measurements of thin Au films on Si/SiO_2 covering the whole spectral range up to 35 000 cm^{-1} (4.3 eV), corresponding to a wavelength of 280 nm. The film thickness d was varied between 3 and 10 nm, i.e., from well below to well above the insulator-to-metal transition.

II. EXPERIMENTAL DETAILS

Thin Au films were prepared by an electron-beam heated effusion cell on commercial 0.55 mm thick Si(100) substrates covered by a 200-nm-thick thermally grown SiO_2 layer. The preparation was performed in ultrahigh vacuum (UHV) at a base pressure of 1×10^{-7} Pa and the substrates were held at room temperature during evaporation. The deposition rate was about 1 Å/min and measured prior to each film deposition by a quartz-crystal microbalance. Keeping the gold flux constant, the film thickness could be controlled by the evaporation time. With a quartz-crystal microbalance, the weight thickness is measured. Since we are interested in the optical properties, we use the effective optical film thickness as determined *ex situ* by ellipsometry[12] throughout the paper. The two quantities are correlated with each other by the filling factor.

All optical experiments were performed at room temperature. The reflectivity measurements in the ir were carried out by a Bruker IFS 66/s Fourier-transform infrared spectrometer in the range of 500–12000 cm^{-1} employing a nitrogen-cooled mercury-cadmium-telluride (MCT) detector. All spectra were recorded with a resolution of 0.5 cm^{-1} and 64 averaged scans. As reference, a thick gold mirror was used. To compare measured spectra to model calculations, etalon effects (multireflection within the substrate) were smoothed out. For the ellipsometry measurements, a Woollam variable-angle spectroscopic ellipsometer (VASE) was utilized. The experiments were carried out in the spectral range between 6000 and 35000 cm^{-1} (0.75–4.3 eV, corresponding to a wavelength of 280 nm to 1.7 μm) with a resolution of 170 cm^{-1} and the angle of incident varied in steps of 5° from 35° to 75°. The dc resistivity of the films was measured by a four-probe van der Pauw method.

III. RESULTS AND ANALYSIS

The thickness-dependent morphology of thin Au films on Si/SiO_2 is well investigated.[9,13] In Fig. 1, atomic force mi-

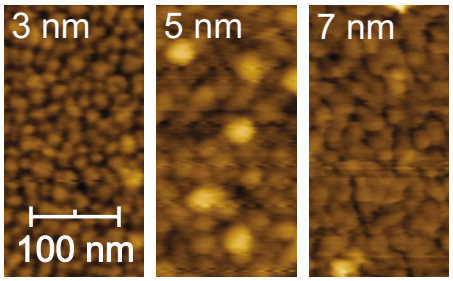

FIG. 1. (Color online) AFM images of 3-, 5-, and 7-nm-thick gold films on Si/SiO_2. All three images are presented at the same scale. With increasing film thickness, the cluster size increases and the films become smoother. For the 7 nm film, the islands are not separated but coalesce to larger clusters.

croscopy (AFM) images of 3, 5, and 7 nm thick gold films at the same scale are presented.[9]

With increasing film thickness, the size of the islands increases, they get closer to each other, and the films become smoother. The AFM image of the 7 nm film shows clearly that the islands of the thicker films coalesce to larger clusters. The percolation threshold itself cannot be determined from the morphology. Although it is important to know the morphology of the films, one has to stress the fact that percolation theories deal with scaling laws and therefore the overall electrical and optical behaviors should be independent on the specific morphology.[7]

Prior to the film preparation, the bare Si/SiO_2 substrates were characterized by ellipsometry and the obtained complex optical parameters $\hat{\epsilon}(\omega)=\epsilon_1(\omega)+i\epsilon_2(\omega)$ then kept fixed in the further modeling of the films. As an example, in Fig. 2, the measured ellipsometric angle Ψ for a 8.1-nm-thick Au film is shown as a function of frequency and angle of incidence. Several attempts were made to model the obtained ellipsometric angles. It was not possible, for instance, to model the granular films by an EMA, even in the case where the volume fraction was gradually decreased over the film thickness. Taking the granular Au layer as a homogeneous effective layer with fixed thickness, it was possible to get

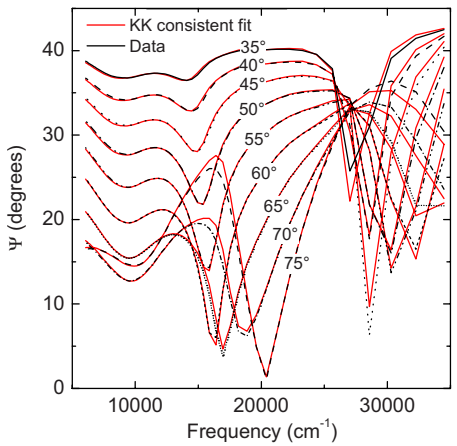

FIG. 2. (Color online) Measured ellipsometric angle Ψ for a 8.1-nm-thick Au film on a Si/SiO_2 substrate for several angles of incidence (dashed lines). Solid lines are the corresponding model fits (for details, see text).

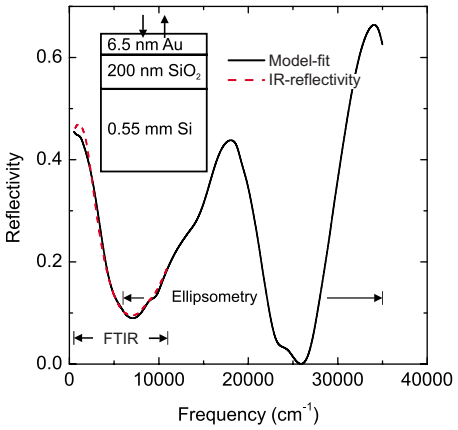

FIG. 3. (Color online) Measured ir reflectivity of a 6.5 nm Au film (dashed line) together with the reflectivity calculated from the Kramers-Kronig consistent dielectric functions obtained by a simultaneous analysis of the ir and ellipsometric data. Inset shows the assumed layer structure.

reasonable agreement to the experimental data by a point-by-point fit with a mean-squared error around 6; but it turned out that the received dielectric functions were not Kramers-Kronig consistent.

To solve this problem, we combined the results obtained by ellipsometry and ir reflectivity. Both sets of data were simultaneously analyzed with the program package REFFIT (for details on this tool, see Ref. 14). By means of a variational dielectric fit within the program, Kramers-Kronig consistent dielectric functions could be obtained, which perfectly reproduces both the ellipsometric angles (continuous line in Fig. 2) as well as the ir reflectivity. In Fig. 3, for example, the measured reflectivity in the ir region (dashed line) of a 6.5-nm-thick Au film with its corresponding fit (solid line) is shown together with the reflectivity up to the uv obtained from the ellipsometric measurement. The dominating oscillation in the reflectivity is due to interferences caused by the 200-nm-thick SiO_2 layer.

The real part $\epsilon_1(\omega)$ of the dielectric function as received from the above analysis is shown in Fig. 4(b) as a function of frequency for varying film thickness. From the imaginary part $\epsilon_2(\omega)$, the optical conductivity[15] was calculated by

$$\sigma_1(\omega) = \omega\epsilon_0\epsilon_2(\omega), \tag{1}$$

with ϵ_0 the permittivity of free space. It is displayed in Fig. 4(a) in a double-logarithmic fashion.

The obtained dielectric functions $\sigma_1(\omega)$ and $\epsilon_1(\omega)$ can be parameterized by a superposition of Drude and Lorentz terms.[15] In Fig. 9, one example of such a deconvolution is shown.

Additionally to the optical characterization, the dc resistivity of the films was measured. In the *in situ* measurement shown in Fig. 5, the sharp transition at the percolation threshold can be seen clearly. The obtained dc-conductivity values for the different thicknesses are included in Fig. 4. They perfectly match with the extrapolated dc values of the optical measurements.

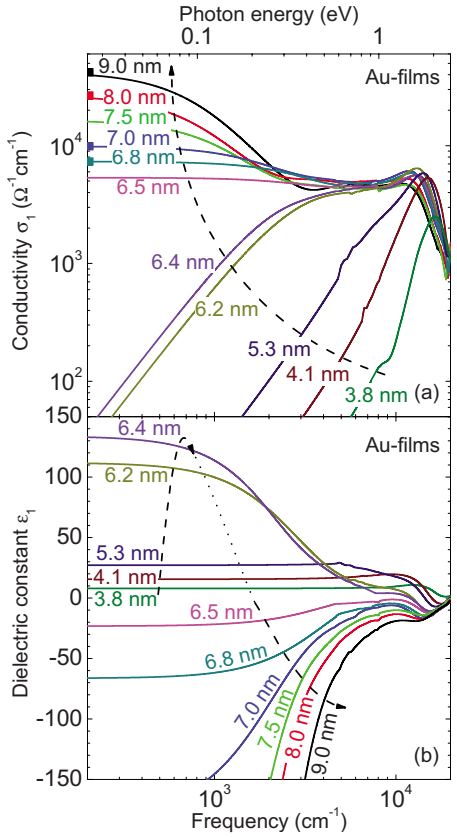

FIG. 4. (Color online) (a) Optical conductivity and (b) dielectric constant of gold films obtained from reflection experiments and ellipsometry at room temperature. The included dc values (solid squares) perfectly match to the extrapolated conductivity $\sigma_1(\omega \rightarrow 0)$. Dashed arrows indicate the tendency as the film thickness increases

IV. DISCUSSION

A. Percolation threshold

From the effective conductivity $\sigma_1(\omega)$ as well as from the effective dielectric function $\epsilon_1(\omega)$ of the gold layers, the different films can be clearly divided in two regimes: the continuous films in the thickness range $d \geq 7$ nm and the granular films with $d \leq 6.0$ nm. The percolation threshold d_c falls right between these two values. The *in situ* dc measurements (see Fig. 5) strongly support this observation.

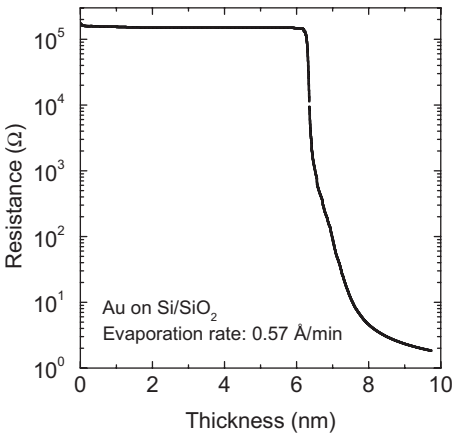

FIG. 5. *In situ* dc-resistivity measurement showing the sharp transition at the percolation threshold. Here the weight thickness is plotted as measured by the quartz microbalance.

Well above the percolation threshold, the conductivity decreases with frequency and the static permittivity $\epsilon_1(\omega \rightarrow 0)$ is negative, both indicating a typical metallic behavior. The low-frequency behavior of the metallic films can be fitted by a simple Drude model[15] with thickness-dependent plasma frequencies ω_p and scattering rates $\gamma = 1/(2\pi c\tau)$. These Drude parameters match perfectly to the directly measured dc conductivity added as dots in Fig. 4. Naturally, the reflectivity of the evaporated films is lower compared to bulk Au because the effective electron density is reduced and the scattering rate γ becomes larger with decreasing film thickness. While the former effect comes from a surface-dipole layer,[16,17] the latter is a well-known consequence of the classical size effect, i.e., it is due to surface scattering and imperfections. Both effects become more pronounced as d is reduced since the surface-to-volume fraction is enhanced.[18–20]

Below the metal-to-insulator transition (MIT) the static conductivity $\sigma_1(\omega \rightarrow 0)$ vanishes and $\epsilon_1(\omega)$ is positive. The optical behavior in this regime can be explained by the absence of the Drude contribution and two resonance peaks in the midinfrared. Below the MIT, we picture metallic islands which interact capacitively. While the dc conductivity is zero, the optical conductivity depends on the capacitive coupling of the islands and thus increases with frequency. From the AFM images of comparable samples (see Fig. 1) and other very extensive studies[13] of the morphology of Au on Si/SiO_2, the thickness dependence can be explained as follows: the metallic clusters are separated from each other forming a condenser. With increasing effective film thickness d, the islands are closer to each other and also larger. While their surface increases, the spacing decreases and tends to zero at the percolation threshold. This leads to a rise of the capacitive coupling and an enhanced optical conductivity (Fig. 4) (for a detailed discussion from a more theoretical point of view, see, e.g., Refs. 21 and 22).

B. Dielectric constant

As far as the thickness dependence of the low-frequency permittivity is concerned, one would expect that ϵ_1, which is positive for $d=0$, gradually decreases with d and becomes negative at the MIT. However, a distinctively different behavior is observed in our experiments. As indicated by the arrow in Fig. 4, $\epsilon_1(\omega)$ first rises with film thickness d, goes through a maximum at some critical thickness d_c which is assumed to be between 6 and 7 nm, and then decreases rapidly; ϵ_1 becomes negative only at considerably larger d, above 7 nm.

In principle, this behavior is known from the low-frequency conductivity of percolating networks. Efros and Shklovskii investigated such systems theoretically and predicted a divergence of the static dielectric constant[22]

$$\epsilon_1(0,d) \propto (d_c - d)^{-s} \tag{2}$$

at a critical thickness d_c. For any small but finite frequency ω, the divergence simply becomes a maximum

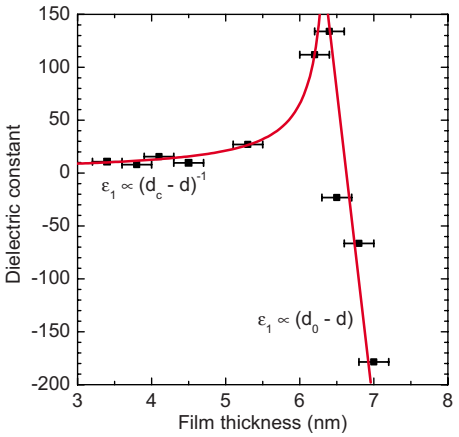

FIG. 6. (Color online) Divergence of the static dielectric constant (obtained at 1 cm^{-1}) as a function of nominal film thickness d for Au on Si/SiO_2. Solid lines below and above d_c correspond to $\epsilon_1(d) \propto (6.4\ \text{nm} - d)^{-1}$ and $\epsilon_1(d) \propto (6.7\ \text{nm} - d)$, respectively.

$$\epsilon_1(\omega, d_c) = \epsilon_s \left(\frac{\sigma_m}{\omega \epsilon_0 \epsilon_s} \right)^{1-u}, \tag{3}$$

where σ_m is the real part of the conductivity of the metallic fraction, $\epsilon_0 = 8.85 \times 10^{-12}$ A s/V m, and ϵ_s the real part of dielectric fraction. For three-dimensional systems, $s=1$ and $u=0.62$ were predicted, while $s=1.3$ and $u=0.5$ for two dimensions.[22] In the case where the conductivity of the insulating fraction cannot be neglected, ϵ_1 saturates at d_c for $\omega \to 0$ at

$$\epsilon_1(\omega \to 0, d_c) = \epsilon_s \left(\frac{\sigma_m}{\sigma_s(0)} \right)^{1-u}, \tag{4}$$

where $\sigma_s(0)$ is the dc conductivity of the dielectric fraction.

Figure 6 exhibits the dielectric constant as a function of film thickness obtained at the extrapolated frequency of 1 cm^{-1}; it represents more or less the static value since ϵ_1 is almost frequency independent below this value. The measurements fit to the expected behavior with a maximum at the critical thickness d_c between 6 and 7 nm. Our data of Au evaporated on Si/SiO_2 below d_c can be best described with $d_c = 6.4$ nm and $s=1$; inferring that a real system of interacting gold nanoparticles should be modeled as a three-dimensional network. Additionally in Fig. 7, the measured maximum $\epsilon_1(\omega, d_c)$ is compared to the values calculated by Eq. (3) assuming $\epsilon_s = 1$ (air). Also, our data do not allow to verify the exact value of u; the large value measured for $\epsilon_1(\omega, d_c)$ exceeds in the entire midinfrared the maximum given by Eq. (3) in two as well as in three dimensions. Here the theory clearly fails to describe the experimental findings. At very low frequencies, $\epsilon_1(\omega \to 0, d_c)$ saturates in agreement with Eq. (4). Whether this is an effect of the non-negligible conductivity of the SiO_2 substrate or has its origin in the fact that we are not exactly at d_c cannot be decided from our measurement. A similar behavior was until now only observed in emulsions.[23]

Until now, we have concentrated on the divergency of ϵ_1. But also σ_1 shows an interesting behavior below d_c, where we picture isolated metallic clusters. While $\sigma_{dc} = 0$, the ac

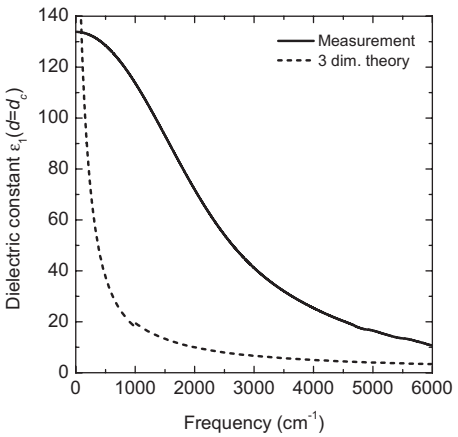

FIG. 7. Comparison between the measured maximum $\epsilon_1(\omega, d_c)$ and the frequency dependence calculated by Eq. (3). Over the entire midinfrared range, the measured values are above the predicted ones. At very low frequencies, the experimental $\epsilon_1(\omega \to 0, d_c)$ saturates.

conductivity depends on the capacitive coupling of the islands and increases with frequency. In the absence of a Drude contribution, it was predicted that $\sigma_1(\omega)$ follows a quadratic frequency dependence $\sigma(\omega) \sim \omega^2$, which can be simulated by a capacitor network.[21,22] This quadratic behavior formulated more than 30 years ago is indeed nicely fulfilled by our Au films as can be seen in Fig. 8.

Another interesting point mentioned in Ref. 22 is observed here in a very nice way. The zero crossing of $\epsilon_1(\omega = 0, d)$ occurs at $d = d_0 \approx 6.7$ nm which falls well above d_c. Since the zero crossing of the dielectric constant is a common measure of metallicity,[15] this implies that the divergence of $\epsilon_1(d)$ does not coincide with the insulator-to-metal transition defined by the zero crossing of $\epsilon_1(d_0)$. Further experiments on other systems are desired to verify and specify this general behavior.

C. Plasmons

For the description of the behavior at higher frequencies, additional Lorentz oscillators have to be considered. To illus-

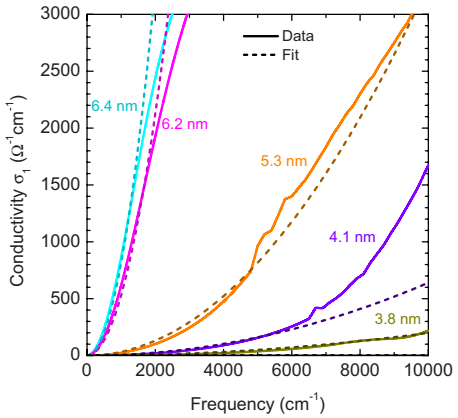

FIG. 8. (Color online) Frequency-dependent conductivity for various Au films below d_c together with the corresponding quadratic fits. In this regime, the films can be pictured as isolated capacitively coupled metal clusters even in the midinfrared.

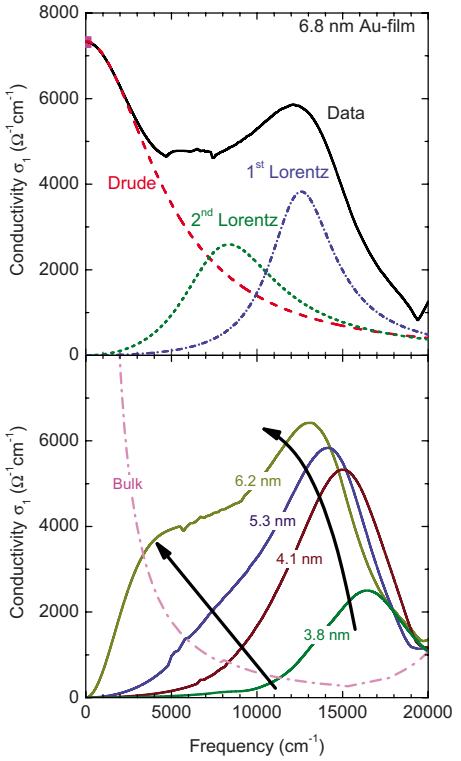

FIG. 9. (Color online) (a) Decomposition of the measured conductivity of the 6.8 nm film in its Drude and Lorentz components. The symbol at $\omega=0$ indicates the independently measured dc value. (b) Development of the two Lorentz oscillators with film thickness. With increasing thickness, both plasmons shift to lower frequencies and the separation between them increases.

trate how the conductivity is built up by the different components, the conductivity is shown in Fig. 9 for the 6.8 nm film together with its different contributions and the independently measured dc value. This film is just above the percolation threshold and exhibits all three contributions very clearly. With increasing film thickness, the two plasmons shift to lower frequencies and become weaker.

In the following, we will first concentrate on the high-frequency mode above 10 000 cm^{-1} caused by the ensemble of single nanoparticles. It is a property of the ensemble and has to be distinguished from free-electron oscillations in isolated metal clusters. The incident electric field is modified by the polarizability of these particles which—most important—interact.[24,25] In literature, this transverse-mode plasmon is referred to as "Maxwell-Garnett resonance" or "optical conduction resonance." It shifts to lower frequencies upon stronger interaction as the metal islands become closer and denser packed. Assuming spherical clusters with a diameter much smaller than the used infrared wavelength, the position of this plasma absorption can be described by the following condition:[24]

$$\epsilon_1^{\text{bulk}}(\omega_p) = -\frac{2+Q}{1-Q}n_s^2. \tag{5}$$

In this condition, Q is the coverage of the substrate, n_s its refractive index, and $\epsilon_1^{\text{bulk}}(\omega)$ is the frequency-dependent dielectric constant of the metallic fraction. If for a given Q the above condition is fulfilled, a plasmon is excited at ω_p. The solid line in Fig. 10 shows the so-calculated resonance frequencies ω_p with $\epsilon_1^{\text{bulk}}(\omega)$ of bulk gold[26] and $n_s=1.45$ for the SiO_2 substrate. The coverage $Q=d_{\text{weight}}/d_{\text{opt}}$ was evaluated from the ratio of the weight and optical thicknesses as determined by ellipsometry and by the deposited mass, respectively.[12] The squares in Fig. 10 are our measured data for the higher-frequency plasmon. The position of this plasmon shifts to lower frequencies with increasing d, closely following the behavior given by Eq. (5); the peak also becomes weaker and broader. Interestingly, the insulator-to-metal transition cannot be discriminated albeit the Maxwell-Garnett theory breaks down above the percolation threshold. For $Q\rightarrow 1$, the plasmon frequency mutates to a Drude peak.

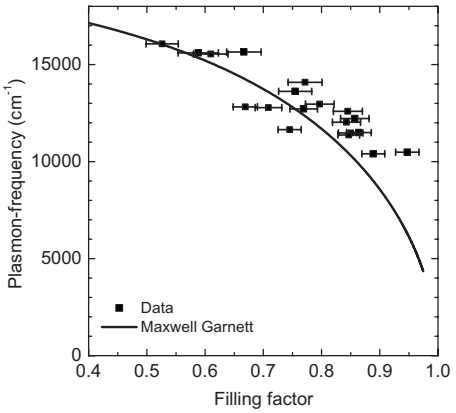

FIG. 10. Comparison between observed and calculated plasmon frequencies. With increasing film thickness, the plasmon frequency drops, closely following the behavior given by Eq. (5).

Ellipsometric studies on thin silver films in the visible and near-infrared spectral ranges are interpreted by de Vries *et al.*[27] as a shift of the localized plasmon to lower frequencies when the films get thicker. Approaching the percolation threshold, the resonance frequency goes to zero and the relaxation time (determined from the Lorentz fit) exhibits an abrupt increase indicating the transition to a macroscopic conducting state. In contrast, our investigations down to very low frequencies clearly evidence the development of a Drude peak and the presence of the plasmon as distinct features. Both exist simultaneously well above the percolation threshold until the plasmon gradually dies out with increasing film thickness d. This can in principle be interpreted in the way that the rough surface of the percolated films still show dipole interaction or that dielectric inclusions in the film start to interact with each other, as it has been considered by Cohen *et al.*[28] It is worthwhile to mention that the measured plasmon mode is broader than the calculated one because the mean-free path of the conduction electrons is limited by the particle size.[24] Size effects also cause a larger scattering rate in the Drude components of the percolated films.

As discussed above, the plasmon referred to as first Lorentz oscillator in Fig. 9 is a property of an ensemble of spherical single clusters. At low coverage, only this peak is seen. At higher coverages, a second peak at lower frequencies appears. In principle, there exist two explanations for

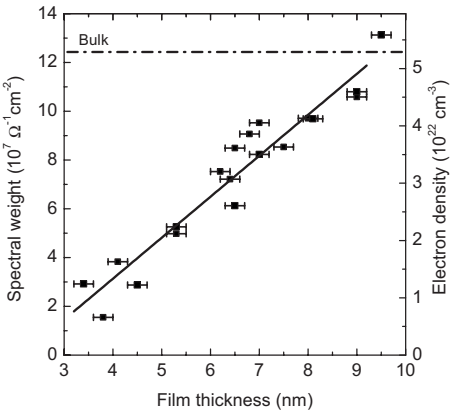

FIG. 11. Spectral weight $\int \sigma_1(\omega)d\omega = \omega_p^2 \pi \epsilon_0/2$ and electron density $N_e = \omega_p^2 \epsilon_0 m/e^2$ of the Drude and the two Lorentz oscillators as function of the film thickness. Dashed line represents the electron density as determined for bulk gold.

this splitting: in prolongate particles, a high-frequency transversal and a lower-frequency longitudinal mode can be observed. Especially at lower coverages, the weak interaction of the Au with the substrate promotes the growth of spherical particles as can be seen from the AFM images, therefore this possibility is not very convincing. The appearance of a second peak can also be an indication for the formation of aggregates.[29] With increasing film thickness, the dipole-dipole interaction between adjacent clusters increases, which also can lead to a splitting of the plasmon resonance into a lower-frequency longitudinal and a high-frequency transversal mode. With increasing coverage, the sample undergoes a transition form statistically ordered separated single clusters to aggregates with various next-neighbor distances. This explains the observation that with increasing film thickness, both plasmon peaks shift to lower frequencies, they broaden, and the splitting between them increases. At the percolation threshold, when additionally the Drude component appears, they cannot be clearly separated anymore (see Fig. 9).

The maximum in $\epsilon_1(\omega)$ at the critical thickness at low frequencies is now a direct consequence of the two competing contributions: below the percolation threshold, the shift of the plasmons to lower frequencies with increasing film thickness leads to an increasing $\epsilon_1(\omega)$. At the percolation threshold d_c, the Drude peak starts to develop, which adds a strong negative component to the dielectric response leading to a maximum in the dielectric function. Eventually, ϵ_1 changes sign at d_0 which is slightly above d_c. This interpretation is supported by the analysis of the spectral weight $\int \sigma_1(\omega)d\omega = \omega_p^2 \pi \epsilon_0/2$ between 0 and 20 000 cm^{-1} and the corresponding electron density $N_e = \omega_p^2 \epsilon_0 m/e^2$ shown in Fig. 11. The spectral weight increases linearly with film thickness reaching the bulk value at about 10 nm. No indication of the MIT between 6 and 7 nm can be identified, i.e., the abrupt change in dc conductivity is not reflected at higher frequencies. There, a monotonous transfer of spectral weight from the plasmons to the Drude peak is observed. The linear increase of the electron density simply describes the growing amount of metal. A similar result for thin silver films was observed by de Vries *et al.*[27]

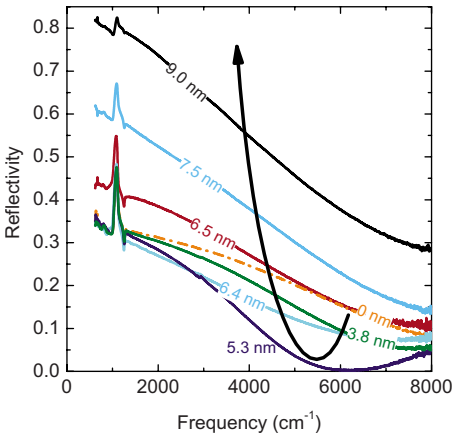

FIG. 12. (Color online) Thickness-dependent reflectivity of Au films on Si/SiO_2. With increasing film thickness, the reflectivity in the infrared first drops below the value of the bare substrate (dashed line), vanishes for a thickness of 5.3 nm around 6000 cm^{-1}, and then increases again reaching the original value of the bare substrate at about the percolation threshold.

D. Suppressed reflectivity

In a previous work, we have shown that nanometer-thick Au layers on Si can act as antireflection coating for infrared light.[9] This effect is a direct consequence of the uncommon behavior of $\epsilon_1(d)$ (see Fig. 6) below the percolation threshold. In Fig. 12, the thickness-dependent reflectivity of the Au films together with the bare Si/SiO_2 substrate is shown. With increasing film thickness, the reflectivity in the infrared first drops below the value of the bare substrate, vanishes for a thickness of 5.3 nm around 6000 cm^{-1}, and then increases again reaching the original substrate value at about the percolation threshold. This behavior can be perfectly modeled using the Fresnel equations for a three-layer system[15] of Au film, 200 nm SiO_2, and Si with the effective Au parameters shown in Fig. 4. The reason for the suppression is not absorption—σ_1 is very small in this range—but the phase shift due to the huge refractive index in this range. In Fig. 13,

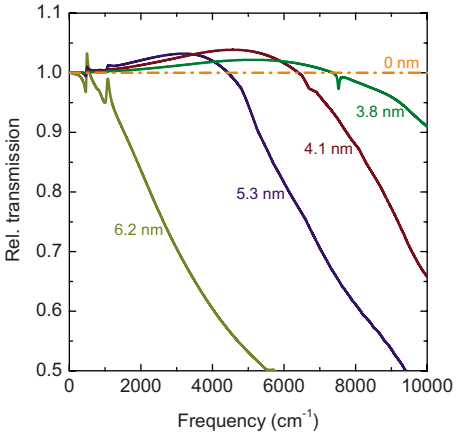

FIG. 13. (Color online) Calculated relative transmission $T_{sub+film}/T_{sub}$ for various film thicknesses below the percolation threshold. Over the entire mid-ir range, the transmission through the Au-covered film is higher than through the bare substrate.

the calculated transmission is also shown. The suppressed reflection results in an enhanced transmission, which exceeds that of the bare substrate over the entire midinfrared range. Nanometer-thick antireflection coatings with metal-cluster films are potential applications for the divergency of the dielectric constant near the percolation threshold.

E. Comparison to Bruggeman

One commonly used model to describe the optical properties of inhomogeneous metal films is the Bruggeman effective-medium approximation (BEMA). It treats the two composites of a cluster film in a symmetric fashion. Therefore, it is in principle able to model the dielectric function of a composite below as well as above the percolation threshold. In the following, we will demonstrate at which point it fails to describe the metal-to-insulator transition itself. In the BEMA, the complex effective dielectric function ϵ_{eff} of a composite built from two materials with the volume fractions Q and $(1-Q)$ and the optical constants ϵ_a and ϵ_b is calculated by

$$Q\frac{\epsilon_a-\epsilon_{\text{eff}}}{\epsilon_{\text{eff}}+L(\epsilon_a-\epsilon_{\text{eff}})}+(1-Q)\frac{\epsilon_b-\epsilon_{\text{eff}}}{\epsilon_{\text{eff}}+L(\epsilon_b-\epsilon_{\text{eff}})}=0. \quad (6)$$

Here, L is the depolarization factor which accounts for the shape of the inclusions. Starting with a spheroid, one can distinguish three extreme cases: $L\rightarrow 0$ corresponds to a rod, $L=1/3$ is a sphere, and $L\rightarrow 1$ is a disk. One drawback of the BEMA is that in this approach, the depolarization factor L is identical with the critical filling factor Q_c at the percolation threshold.[6] In our case, Q_c is about 0.75. This corresponds to very flat ellipsoids, which roughly reflects the shape of our clusters. To compare the experimental values (see Fig. 4) to that calculated with Eq. (6), the filling factor Q was chosen so that the experimental and calculated $\epsilon(\omega)$ values coincide at $\omega\rightarrow 0$. As can be seen from Fig. 14 for very thin films, the BEMA model can describe the experimental values up to the midinfrared, but there are strong deviations at higher frequencies even for the thinnest film. With increasing film thickness, the agreement becomes even worse mainly due to the fact that neither the position nor the strength of the plasmon is correctly reproduced by the BEMA model. The metal-to-insulator transition itself is reproduced by the calculations but the transition is much too sharp and the high-frequency conductivity above the transition is overestimated. The slowly dying plasmon above the percolation threshold is totally absent in the BEMA model. A general problem of all effective-medium approximations is that their results not necessarily fulfill this important causality condition.[6] We want to stress one important additional point not shown in Fig. 14: our experimentally obtained complex dielectric functions displayed in Fig. 4 are Kramers-Kronig consistent.

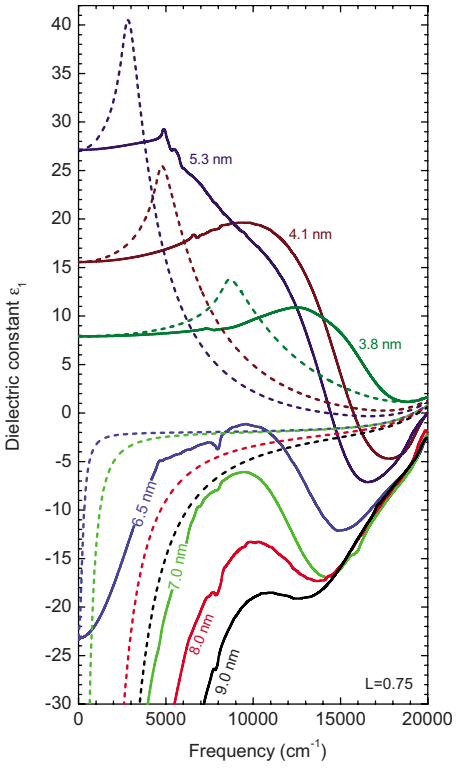

FIG. 14. (Color online) Comparison between the measured effective ϵ_1 and the calculated one using Eq. (6) (dashed lines). The BEMA model can reproduce the experimental values only at very low coverage and low frequency.

V. CONCLUSION

Combining infrared spectroscopy, spectroscopic ellipsometry, and dc measurements, the effective dielectric function of thin Au films around the percolation threshold could be obtained over a very broad frequency range up to the ultraviolet. The optical properties of the films can in principle be described by two contributions: two plasmon peaks in the near infrared, which shift down with increasing film thickness and slowly die out above the MIT, and a Drude peak, which starts to develop at the MIT and then rapidly increases with film thickness. The interplay of both components leads to a dielectric anomaly, known from percolation theory: from dc up to a few thousand wave numbers, $\epsilon_1(\omega)$ exhibits a pronounced maximum at some critical thickness. Whereas percolation theory roughly describes the optical anomaly around the metal-to-insulator transition, effective-medium approximations give reasonable results only far away from the percolation threshold.

[1] H. E. Bennett and J. M. Bennett, in *Optical Properties and Electronic Structure of Metals and Alloys*, edited by F. Abelès (North-Holland Publishing Company, Amsterdam, 1966).
[2] T. J. Coutts, *Electrical Conduction in Thin Metal Films* (Elsevier, Amsterdam, 1974), and references therein.
[3] G. Fahsold, A. Bartel, O. Krauth, N. Magg, and A. Pucci, Phys. Rev. B **61**, 14108 (2000).
[4] J. C. M. Garnett, Philos. Trans. R. Soc. London **203**, 385 (1904).
[5] D. A. G. Bruggeman, Ann. Phys. **416**, 636 (1935).
[6] T. C. Choy, *Effective Medium Theory* (Clarendon Press, Oxford, 1999).
[7] J. P. Clerc, G. Giraud, J. M. Laugier, and J. M. Luck, Adv. Phys. **39**, 191 (1990).
[8] Y. Yagil, P. Gadenne, C. Julien, and G. Deutscher, Phys. Rev. B **46**, 2503 (1992).
[9] B. Gompf, J. Beister, T. Brandt, J. Pflaum, and M. Dressel, Opt. Lett. **32**, 1578 (2007).
[10] U. Kreibig and M. Vollmer, *Optical Properties of Metal Clusters* (Springer, New York, 1995).
[11] D. Bedeaux and J. Vlieger, *Optical Properties of Surfaces* (Imperial College Press, London, 2002).
[12] H. Schopper, Fortschr. Phys. **2**, 275 (1954).
[13] S. Pal, M. K. Sanyal, S. Hazra, S. Kundu, F. Schreiber, J. Pflaum, E. Barrena, and H. Dosch, J. Appl. Phys. **95**, 1430 (2004).
[14] A. Kuzmenko, Guide to REFFIT: software to fit optical spectra (2007), http://optics.unige.ch/alexey/reffit.html
[15] M. Dressel and G. Grüner, *Electrodynamics of Solids* (Cambridge University Press, Cambridge, England, 2002).
[16] N. D. Lang, in *Solid State Physics*, edited by H. Ehrenreich, F. Seitz, and D. Turnbull (Academic Press, New York, 1973), Vol. 28, p. 228.
[17] F. K. Schulte, Surf. Sci. **55**, 427 (1976).
[18] A. Pucci, F. Kost, G. Fahsold, and M. Jalochowski, Phys. Rev. B **74**, 125428 (2006).
[19] M. Walther, D. G. Cooke, C. Sherstan, M. Hajar, M. R. Freeman, and F. A. Hegmann, Phys. Rev. B **76**, 125408 (2007).
[20] T. Brandt, M. Hövel, B. Gompf, and M. Dressel, Phys. Rev. B **78**, 205409 (2008).
[21] V. E. Dubrov, M. E. Levinshtein, and M. S. Shur, Zh. Eksp. Teor. Fiz. **70**, 2014 (1976) [Sov. Phys. JETP **43**, 1050 (1976)].
[22] A. L. Efros and B. I. Shklovskii, Phys. Status Solidi B **76**, 475 (1976).
[23] M. A. van Dijk, G. Casteleijn, J. G. H. Joosten, and Y. K. Levine, J. Chem. Phys. **85**, 626 (1986).
[24] R. H. Doremus, J. Appl. Phys. **37**, 2775 (1966).
[25] J. P. Marton and J. R. Lemon, Phys. Rev. B **4**, 271 (1971).
[26] Bulk-Au data were measured with Fourier-transform infrared spectroscopy and ellipsometry on different bulk samples. The used data are very similar to *Handbook of Optical Constants of Solids*, edited by E. D. Palik (Academic Press, Orlando, 1985), but in contrast to the literature values, our data do not show any jumps in the whole frequency range.
[27] A. J. de Vries, E. S. Kooij, H. Wormeester, A. A. Mewe, and B. Poelsema, J. Appl. Phys. **101**, 053703 (2007).
[28] R. W. Cohen, G. D. Cody, M. D. Coutts, and B. Abeles, Phys. Rev. B **8**, 3689 (1973).
[29] U. Kreibig, M. Quinten, and D. Schoenauer, Phys. Scr. **T13**, 84 (1986).